A Programmable Biopotential Aquisition Front-end with a Resistance-free Current-balancing Instrumentation Amplifier

Paul FARAGÓ[1], Robert GROZA[1], Sorin HINTEA[1], Peter SÖSER[2]
[1]*Technical University of Cluj-Napoca, 400114, Romania*
[2]*Graz University of Technology, 8010, Austria*
paul.farago@bel.utcluj.ro

***Abstract*—The development of wearable biomedical equipment benefits from low-power and low-voltage circuit techniques for reduced battery size and battery, or even battery-less, operation. This paper proposes a fully-differential low-power resistance-free programmable instrumentation amplifier for the analog front-end of biopotential monitoring systems. The proposed instrumentation amplifier implements the current balancing technique. Low power consumption is achieved with subthreshold biasing. To reduce chip area and enable integration, passive resistances have been replaced with active equivalents. Accordingly, the instrumentation amplifier gain is expressed as the ratio of two transconductance values. The proposed instrumentation amplifier exhibits two degrees of freedom: one to set the desired range and the other for fine-tuning of the voltage gain. The proposed IA is employed in a programmable biopotential acquisition front-end. The programmable frequency-selective behavior is achieved by having the lower cutoff frequency of a Gm-C Tow-Thomas biquad varied in a constant-C tuning approach. The proposed solutions and the programmability of the operation parameters to the specifications of particular bio-medical signals are validated on a 350nm CMOS process.**

***Index Terms*—analog processing circuits, biomedical monitoring, biomedical signal processing, operational amplifiers, programmable circuits.**

I. INTRODUCTION

Recent trends in the semiconductor industry guide the circuit development process towards low-power and low-voltage integrated circuits. Specific low-voltage and low-power circuit techniques, such as charge pumps, bulk terminal biasing, bulk terminal input, subthreshold operation, etc. [1, 2] have enabled the portability of a wide range of applications, ranging from consumer electronics to communications and healthcare.

In biomedical electronics, the low-voltage and low-power trends target the development of battery-operated, or even battery-less, wearable medical equipment for in-vivo monitoring and stimulation of the human tissue [1]. Examples of applications which nowadays gain considerable attention are: brain-computer interface systems, insulin pumps, pacemakers, auditory prostheses, bio-potential monitoring systems, non-invasive cerebrovascular monitoring, etc. [2-7].

Biomedical monitoring systems operate towards the acquisition of the bio-potentials of the human body [3]. Although signal processing in bio-medical monitoring systems is mostly digital, bio-potential acquisition and some pre-processing in terms of amplification and filtering is analog. Large-gain high-precision amplification in biomedical monitoring systems is implemented with an instrumentation amplifier (IA). Signal preconditioning and some artifact removal, prior to analog-to-digital conversion, is performed with analog filters. As such, biomedical monitoring systems can strongly benefit from low-power and low-voltage circuit techniques to improve equipment portability and lengthen battery lifetime.

One step forward, wide-range parameter programmability is a key factor for optimizing the operating performance of integrated electronics. For the specific case of bio-potential monitoring systems, the programmability feature can be used to adapt the operation parameters, in terms of gain and bandwidth, to the particular specifications of the targeted bio-potential. For exemplification, the amplitude and frequency specifications for some biopotentials are listed in Table I [8, 9].

TABLE I. AMPLITUDE AND BASEBAND SPECIFICATIONS FOR SOME BIOMEDICAL SIGNALS

Bio-potential	Amplitude range	Baseband frequency
Electrocardiogram (ECG)	100μV - 10mV	0.05Hz - 100Hz
Electroencephalogram (EEG)	10μV - 100μV	0.1Hz - 50Hz
Electromyogram (EMG)	1μV - 10mV	20Hz - 2kHz
Electroneurogram (ENG)	0.1μV - 10μV	500Hz - 10kHz
Electrooculogram (EOG)	10μV - 1mV	DC - 100Hz
Electroretinogram (ERG)	1μV - 1mV	DC - 50Hz

The specified amplitude range and baseband frequency of the bio-potential signals state the requirement for large voltage gain values, as well as low frequency filtering. Common solutions for amplification and filtering employ passive components [8], which limit integration and programming.

In this paper we propose a low-power resistance-free programmable IA for use in the analog front-end of a bio-potential monitoring systems. The proposed IA is built around the current balancing technique, and enables integration and parameter programming by replacing the passive resistances with active equivalents. Given the very low baseband frequency however, passive capacitors cannot be avoided. Therefore, we have employed a constant-C tuning approach for programming the frequency behavior internally to the IA.

The results presented in this paper were obtained with the support of the Technical University of Cluj-Napoca through the research Contract no. 2000/12.07.2017, Internal Competition CICDI-2017.

Digital Object Identifier 10.4316/AECE.2018.02011

This paper is organized as follows. Section 2 presents a review of IA solutions proposed in literature and describes the current balancing technique employed in IAs. Section 3 describes the proposed programmable resistance-free instrumentation amplifier with frequency-selective behavior. Next, Section 4 presents the employment of the proposed IA in the analog front-end of a biopotential monitoring system. Results are presented in Section 5 to validate the proposed solutions.

II. Related Work

The requirements for instrumentation amplifiers are expressed in terms of high input impedance, low input-referred noise, low offset voltage, high differential gain, high common-mode rejection ratio (CMRR) and high power supply rejection ratio (PSRR) [3, 10].

A general solution for IAs is the pre-amplifier - difference amplifier configuration [11], illustrated in Fig. 1.

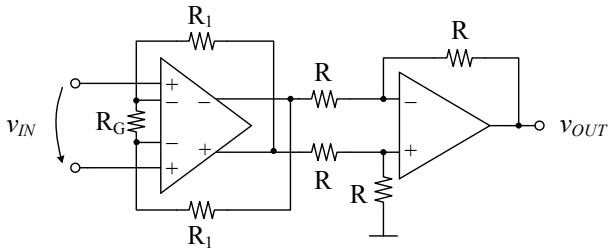

Figure 1. Block diagram of the pre-amplifier - difference amplifier configuration for instrumentation amplifiers

The most common implementation of the IA configuration in Fig. 1 assumes three operational amplifiers (OpAMP) with resistive feedback. The pre-amplifier stage sets the IA gain as the ratio of two resistance values, followed by the difference amplifier which operates differential to single-ended conversion. The IA gain is then expressed as a resistance ratio [11]

$$A_V = 1 + \frac{2R_1}{R_G} \tag{1}$$

This configuration is implemented in many commercially available instrumentation amplifiers, e.g. the AD62X, AD82XX, AD855X series from Analog Devices [11]. An alternative IA with the 3-OpAMP configuration, which employs passive capacitors instead of resistors to set the IA gain, was proposed by Fay et al. in [12]. Subthreshold biasing of the amplifiers in this case lowers the power consumption. Also, the employment of passive capacitors rather than resistors enables integration.

In either IA solution based on the pre-amplifier - difference amplifier configuration, precise matching of the passive components is mandatory for high CMRR, and consequently proper IA operation.

In order to implement a high CMRR, the IA can be extended with the employment of the chopper stabilization technique [13], which is illustrated in the block diagram from Fig. 2.

Chopper stabilization is typically employed for offset and drift suppression, yet it has also been successfully employed for biomedical applications [14]. The input signal is applied to a switch modulator driven by a chopper frequency clock signal f_{chop}. The modulated signal is then amplified, followed by demodulation and lowpass filtering (LPF). For exemplification, a chopper stabilized IA was developed by Hsu et al. for the monitoring of ECG signals [15].

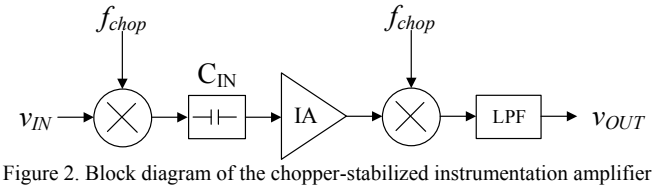

Figure 2. Block diagram of the chopper-stabilized instrumentation amplifier

The advantages of employing chopper stabilization for the implementation of IAs are high CMRR, high accuracy, low drift, suppression of low-frequency noise with low signal aliasing and can achieve rail-to-rail input operation [14]. Accordingly, chopper-stabilized IAs are very well suited for acquisition of EEG biopotentials. Indeed, Huang et al. employed a chopper stabilized IA for the acquisition of EEG signals [16]. Wu et al. on the other hand employed chopper-stabilized IAs for the development of an 8-channel EEG acquisition front-end [17]. Other examples of employment of the chopper stabilized IA accounts to Denison et al. for the chronic measurement of neural field potentials [14], or to Kim et al. who developed a low-power and low-noise dynamic IA for biopotential acquisition [18].

For improved IA performance, chopper stabilization can be employed in conjunction with auto-zero schemes [19], [20], i.e. the switched capacitor C_{IN} in Fig. 2. For exemplification, Guesa et al. developed a switched-capacitor chopper-notch modulator for replica image cancelation in chopper amplifiers [21]. Another example of implementing the switched-capacitor technique in IAs accounts for the commercially available LTC1043 [22].

An alternative solution for IA implementation is the current balancing technique [9-10], [23] illustrated in Fig. 3.

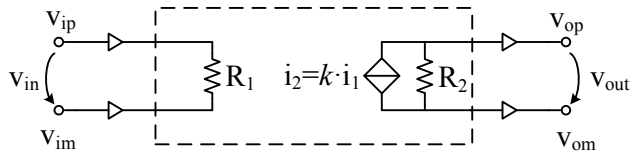

Figure 3. Block diagram of the current-balancing instrumentation amplifier

The differential input voltage v_{in} generates a current through resistor R_1, expressed as

$$i_1 = v_{in} / R_1 \tag{2}$$

The current i_1 is copied to the output section with a current gain factor k, thus

$$i_2 = k \cdot i_1 \tag{3}$$

The current i_2 generates a voltage drop on resistance R_2, which provides the differential output voltage expressed as

$$v_{out} = i_2 \cdot R_2 = k \cdot i_1 \cdot R_2 = k \cdot \frac{v_{in}}{R_1} \cdot R_2 \tag{4}$$

Then, the voltage gain of the instrumentation amplifier is

$$A_V = \frac{v_{out}}{v_{in}} = k \cdot \frac{R_2}{R_1} \tag{5}$$

The typical CMOS implementation of the current-balancing IA assumes the buffered input and output stages from Fig. 3 implemented with a differential pair each, with a passive resistance deployed between the transistor sources.

A differential input voltage, sensed by passive resistance R_1, will cause an imbalance of the differential input pair. Negative feedback is then applied via a transconductance amplifier to bring the input differential pair to equilibrium. The same transconductor output current is sourced into the IA output stage, thus determining a voltage drop on R2. Overall, the IA implements the transfer function expressed in (5). This procedure has been implemented by Martens et al. for IA development of a portable EEG acquisition systems [24]. Another illustration of this procedure was described by Nanda et al. for the development of a portable ECG monitoring system [25]. Implementation of the programmability feature on this current balancing IA structure was described by Huang et al. in [9], as well as in our previous work [26].

A current balancing IA which reduces the implementation complexity and drops the transconductance amplifier for the implementation of negative feedback was described by Wu et al in [27]. Alternatively, Steyaert et al. illustrated an implementation of a current-balancing instrumentation amplifier with a single differential stage [28].

The advantage of the current-balancing IA is that its transistor-level implementation allows for integration in application specific integrated circuits (ASIC). Accordingly, the IA can be integrated on the same silicon dye along with latter analog signal processing sections, e.g. programmable gain sections [4] and analog filters [29], for the silicon implementation of the biopotential acquisition front-end. An ASIC example accounts for Garje et al. who developed a high CMRR bio-circuit for ECG signal monitoring around the current-balancing IA structure [30].

For improved CMRR performance, the current balancing IA can also be deployed in conjunction with chopper stabilization, as illustrated by Huang et al. for portable biopotential acquisition [31].

III. The Proposed Instrumentation Amplifier

The current balancing technique is indeed a versatile approach for IA implementation. Gain setting is straightforward by adjusting the ratio of two resistance values, and high CMRR is inherently achieved by avoiding the severe requirement for passive component matching. Also, if the IA is properly biased in subthreshold, very small power consumption is obtained.

Several issues however need to be addressed for subthreshold biasing. In subthreshold operation, usual current levels are tens to hundreds of nA. Resistance values are therefore in the MΩ order of magnitude, making the solution unfeasible for integration in silicon. External resistors are usually required, and IA gain is consequently limited by the available discrete resistors. Moreover, digital gain programmability becomes impractical in this situation.

In this paper we aim to address these implementation issues in order to develop a resistance-free fully integrated current-balancing IA which enables parameter tuning in either analog or digital fashion. The transistor-level schematic of the proposed IA is illustrated in Fig. 4 and is explained as follows. Bulk-input PMOS transistors M_{ina} and M_{inb} were used as input differential pair, for low flicker noise and linearity [3], [25].

Aiming to compensate for the issue of large passive resistances when implementing subthreshold biasing, we have developed a resistance-free IA solution. Therefore, resistance R_1 from Fig. 3 is implemented with transistor M_{dr} biased in linear region. To be noticed is that in typical implementations of the current-balancing IA schematic, the passive resistance R_1 doesn't count for linearization but rather for acquisition of the differential input voltage [24], [26]. In the proposed work however, we target linearization of the input stage via source degeneration. Accordingly,

$$R_1^{eq} >> 1/G_{in} \tag{6}$$

where R_1^{eq} is the equivalent resistance of M_{dr}, and G_{in} is the transconductance of the input transistors. Consequently, the input transconductance is expressed as

$$G_1 \cong 1/R_1^{eq} \tag{7}$$

which accounts for the gain of the voltage to current conversion by the input stage.

In the IA output stage, we have employed a fully differential operational transconductance amplifier (OTA) G_2 with negative feedback for the active simulation of R_2. Thus, the equivalent resistance value is given by

$$R_2^{eq} = 1/G_2 \tag{8}$$

Replacing expressions (7) and (8) in (5) gives the IA gain as the ratio of two transconductance values, expressed as

$$A_v = G_1 / G_2 \tag{9}$$

The proposed implementation of the current balancing principle in the proposed IA is based on the solution described in [27] and is explained as follows. The output current of the input transconductance stage is applied to a folded-cascode stage M_1-M_4. The folded-cascode stage

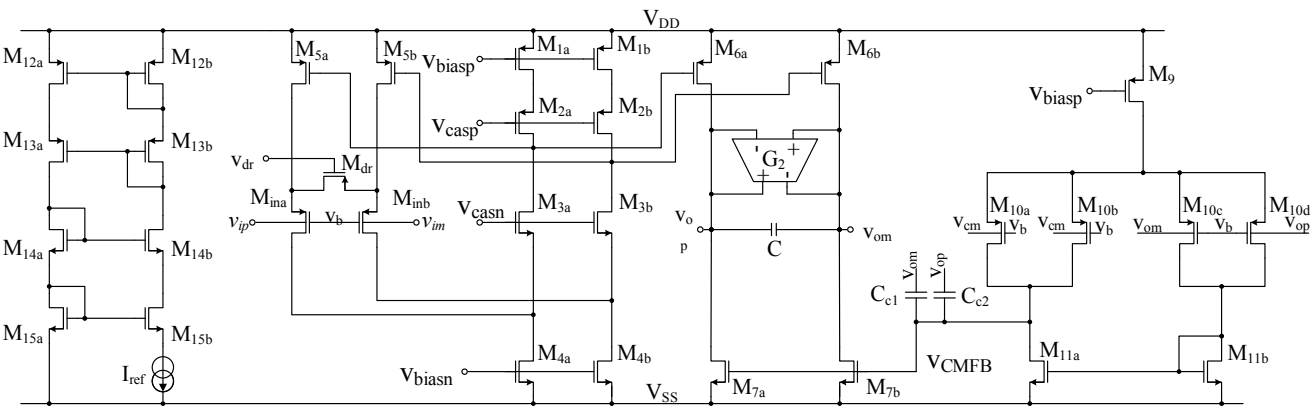

Figure 4. Transistor-level schematic of the proposed programmable resistance-free current-balancing instrumentation amplifier

differential output voltage drives the bias transistors M_5 in a negative feedback configuration. This generates a small-signal current which aims to drive the input transconductance stage to equilibrium, by balancing the bias currents of the input differential pair. The same small-signal current is generated in the drains of transistors M_6, i.e. in the IA output stage, with an additional current gain factor k which can be implemented at this point.

To be noticed is that, unlike the solutions proposed in [9], [10] and [23], [25], we skip differential - to - single-ended conversion in the IA output stage and maintain the differential nature of the output signal in order to perform further analog signal processing in a fully differential fashion.

The common-mode feedback (CMFB) amplifier is implemented with transistors M_9-M_{11}, which actually resembles a single-ended difference amplifier. The error measuring the difference between the IA output common-mode voltage, applied to M_{10a} and M_{10b}, and the reference common-mode voltage (V_{CM}) applied to M_{10c} and M_{10d}, is amplified in order to drive the gates of the bias transistors M_7. The negative feedback loop thus balances differential signal of the folded-cascode output around the reference DC level. Capacitances C_{c1} and C_{c2} compensate the CMFB loop for stability [32].

The bias circuit implemented with current source I_{ref} and transistors M_{12}-M_{15} generate the required gate voltages to bias the transistors in the IA structure [3]. Alternatively, one could employ a self-biasing scheme as described in [33].

Finally, passive capacitance C connected between the IA output pins operates towards band limitation in terms of a lowpass filter [24], [25], [28]. In a similar fashion, a passive inductance connected between the IA output pins would operate towards band limitation in the shape of a highpass filter. This achieves IA band limitation to the biopotential baseband specifications listed in Table I.

Rather than employing a passive inductance for tuning the IA frequency band to the specifications of the biopotentials being monitored, in this work we adopt a solution based on a tunable bandpass filter, as will be illustrated in the next section.

Programmability of the proposed IA is discussed as follows. Active source degeneration in the input differential pair was implemented with the switched array of parallel transistors illustrated in Fig. 5. Provided a fixed resistance value $1/G_2$ in the IA output stage, the parallel transistor array was designed to switch the IA voltage gain between three reference values: x1, x10 and x100 respectively, by digital control word $[a_2a_1a_0]$.

The OTA from the IA output stage, resembling an active resistance, is implemented with the binary weighted transconductor array illustrated in Fig.6 (a) [32]. This topology realizes an equivalent transconductance value expressed as the binary weighted sum of a unit transconductance G_{mu} given by

$$G_m = G_{mu}\left(1+\sum_{i=0}^{2} b_i \cdot 2^i\right) \tag{10}$$

Accordingly, digital tuning of the OTA transconductance is performed in a via digital control word $[b_2b_1b_0]$.

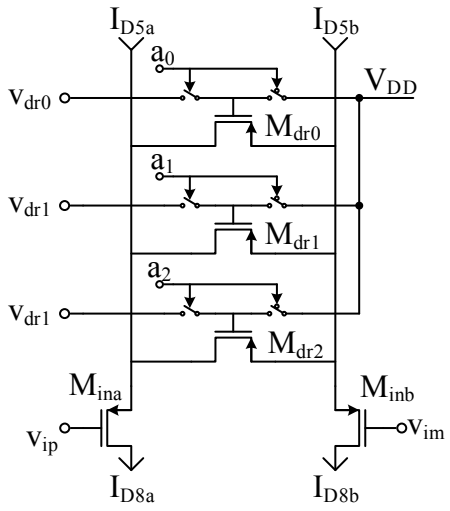

Figure 5. Schematic of the switched array of parallel transistors

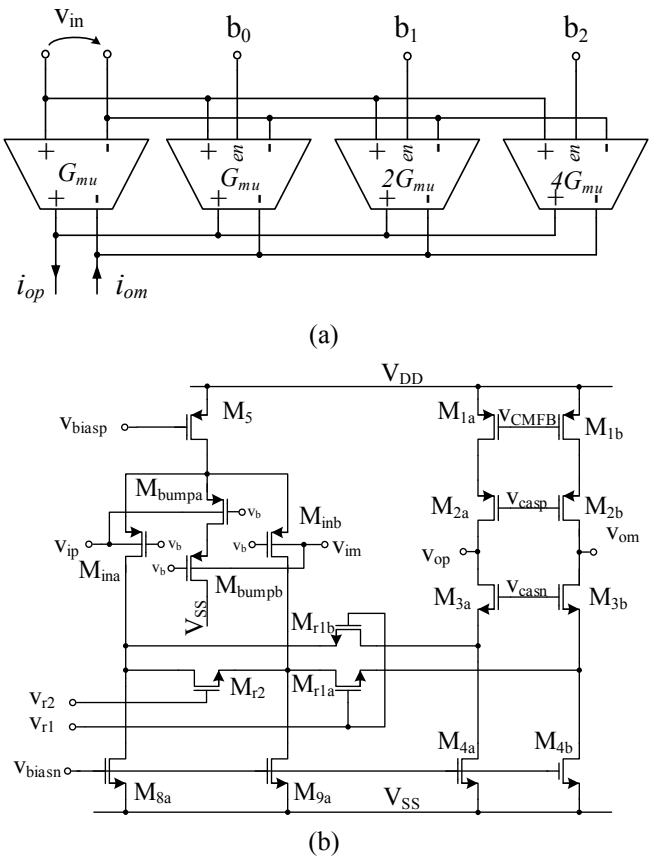

Figure 6. Schematic of the (a) binary weighted transconductor array, and (b) transistor-level implementation of the unit operational transconductance amplifier

The transistor-level schematic of the unit transconductor with folded-cascode load is illustrated in Fig. 6 (b). The transconductor must exhibit sufficient linear range to accommodate the IA output voltage swing. Therefore, the variation of the IA output voltage had to be considered. For example, for EEG signal monitoring, the IA input signal reaches up to $200\mu V^{p-p}$. Assuming a gain factor of 100, the IA output signal may reach $20mV^{p-p}$. Similarly, the maximum $20mV^{p-p}$ ECG input signal with a gain factor of 25 translates to a $500mV^{p-p}$ variation of the IA output. In order to accommodate the required linear range, the OTA from Fig. 3 (b) is linearized with bulk input - M_{in}, and bump linearization - M_{bump} [34].

Transistors M_{r1} and M_{r2} biased in the linear region implement a current divider which realizes transconductance tuning expressed as [32]

$$G_{mu}^{*} = \alpha \cdot G_{mu} \tag{11}$$

where α is the current division factor and is expressed with the transistor aspect ratios and bias voltages as [29]

$$\alpha = \frac{\dfrac{L_{r2}}{\mu C_{ox} W_{r2}(V_{DA} - V_{r2} - Vth)}}{\dfrac{L_{r2}}{\mu C_{ox} W_{r2}(V_{DA} - V_{r2} - Vth)} - \dfrac{L_{r1}}{\mu C_{ox} W_{r1}(V_{DA} - V_{r1} - Vth)}} \tag{12}$$

The parameters in (12) are as follows: μ, C_{ox} and V_{th} are process parameters and represent the charge mobility, oxide capacitance and threshold voltage respectively, W and L are the width and length of transistors M_{r1} and M_{r2}, as indicated by the subscripts, and V_{DA} is the voltage in the drain of transistor M_{ina}.

Starting from the IA reference gain, the equivalent transconductance value G_2 implemented with the transconductor array and expressed with (10), will adjust the IA voltage gain to the desired level according to (9). For fine-tuning, having transistor M_{r2} implemented with a parallel transistor array similar to Fig. 5, achieves digital programming of the IA voltage gain. Differential-mode control voltage

$$V_{cd} = V_{r1} - V_{r2} \tag{13}$$

then achieves analog tuning as expressed in (11).

IV. Analog Front-end for Biopotential Monitoring Systems

The electrical schematics of the biopotential monitoring system analog front-end is illustrated in Fig. 7 and is explained as follows.

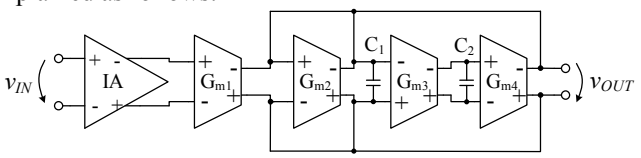

Figure 7. Analog front end for a biopotential monitoring system

Capacitors C_1 and C_2 and transconductors G_{m1}, G_{m2}, G_{m3} and G_{m4} implement a bandpass Tow-Thomas biquad. Capacitances C_1 and C_2 implement the frequency-selective behavior of the biopotential monitoring front-end as follows. Capacitance C_1 implements frequency limitation in terms of an upper cutoff frequency. The gyrator-capacitance structure G_{m3}, G_{m4} and C_2 implements frequency limitation in terms of a lower cutoff frequency.

The limits of the targeted frequency bandwidths are in the DC/0.01Hz - 10kHz range. Even though the IA and the OTAs are biased in subthreshold, the capacitance values are rather large i.e. 470pF and 800nF for the upper and lower cutoff frequencies respectively. The capacitors are thus unsuitable for integration and external components are required to implement the desired frequency-selective characteristics.

Given the high capacitance values, which require external components, we have adopted a constant-C tuning approach [35], which keeps the capacitance value fixed and varies only the transconductance.

To be noticed in Table I is that, while the upper cutoff frequency only exhibits a few distinct values, the lower cutoff frequency covers a much larger variation range. Thus, only the lower cutoff frequency was considered for soft programming. This motivates our choice for the Tow-Thomas biquad structure, as it enables independent tuning of the lower cutoff frequency as a function of the transconductance value in the constant-C tuning technique.

Provided the transconductors G_{m1} - G_{m4} are implemented with the operational transconductance amplifier from Fig. 6, the biopotential monitoring analog front-end allows both digital programming and analog fine-tuning of the operation parameters. Accordingly, in the proposed implementation of the constant-C tuning technique, switching the binary weighted transconductor arrays G_{m3} and G_{m4} sets the frequency range, while variation of the unit transconductance via the current divider $M_{r1\_Gm3,4}$-$M_{r2\_Gm3,4}$ implements fine-tuning of the lower cutoff frequency, following equation

$$f_{cL} = -\frac{G_{m2}}{4\pi C_1} + \frac{1}{2\pi}\sqrt{\frac{G_{m2}^{2}}{4C_1^{2}} + \frac{G_{m3}G_{m4}}{C_1 C_2}} \tag{14}$$

V. Results

The proposed resistance-free IA with programmable frequency-selective behavior was designed for subthreshold operation with a 1.6V asymmetrical supply. The transistor-level schematic was implemented in Cadence using the AMS 0.35µm technology. Results obtained with Virtuoso proves the functionality of the proposed IA solution.

The OTA was designed for a unit transconductance value G_{mu} of 200nS. The performance parameters of the unit transconductor are listed in Table II.

Table II. Simulated Performance Parameters of the Unit Transconductor

Parameter	Value
Supply current	1.17 µA
Input common mode range	-100 mV - 1.3 V
Unit transconductance	200 nS
Linear range	500 mV^{p-p}
3dB bandwidth	60 kHz
THD@10Hz, Vin=10mV^{p-p}	-57dB
THD@10Hz, Vin=1mV^{p-p}	-71dB
Power consumption	1.87 µW

The IA performance parameters are then listed in Table III. For comparison, the performance measures of some IAs reported in literature were also listed in Table III. As illustrated, the proposed IA in this work requires a considerably lower supply current absorption. With the 1.6V supply voltage, this leads to a lower power consumption in comparison to other solutions proposed in literature. Moreover, the common-mode rejection ratio (CMRR), noise performance and offset can be improved even further by deploying the proposed IA in conjunction with the chopper stabilization technique.

Further on, the programmability of the IA voltage gain is illustrated. The x1, x10 and x100 reference IA voltage gain levels, set by switching the active source degeneration transistor M_{dr}, are illustrated in the IA voltage transfer characteristics in Fig. 8. As illustrated, both x10 and x100

TABLE III. SIMULATED PERFORMANCE PARAMETERS OF THE INSTRUMENTATION AMPLIFIER

Parameter	[12]	[11] EEG	[14]	[7]	[13] ECG	This work
Technology	3 µm	n. a.	0.35 µm	0.35 µm	0.18 µm	0.35 µm
Supply voltage	±2.5 V	±4.5 V	1V	±1.5 V	1V	1.6 V
Supply current	31 µA	520 µA	50 µA	47.4 µA	165 µA	4.3 µA
Input common mode range	-1.12 – 0.76 V	n. a.	0.68 – 1.2 V	-1.4 – 0.33 V	-50 – 650 mV	-0.1 – 1.3 V
Voltage gain	programmable, max. 40 dB	programmable, max. 40 dB	43 dB	80 dB	45.5 dB	programmable, max. 60dB
Bandwidth	570 Hz	150 Hz	0.4 Hz – 35 kHz	n.a.	150 Hz	programmable, 0.01 Hz → 40 kHz
CMRR@0.05Hz→200Hz	> 70 dB	99 dB	106 dB	155 dB	127.3 dB	103 dB
PSRR@0.05Hz→200Hz	> 50 dB	40 dB	73.5 dB	131 dB	n.a.	87 dB

reference IA gains exhibit sufficient input linear range to accommodate the biopotential amplitude ranges with the required voltage gain.

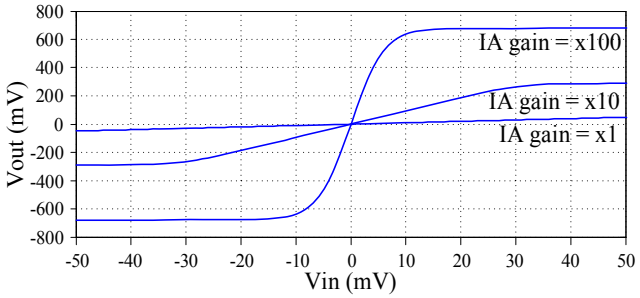

Figure 8. IA voltage transfer characteristics illustrating the x1, x10 and x100 reference gains respectively

For the x10 reference gain value, variation of the IA voltage gain with the transconductance G_2 is illustrated in Fig. 9 as follows. The voltage transfer characteristics are plotted in Fig. 9 (a) for values of G_{m2} ranging from G_{mu} to $8G_{mu}$. The IA gain programming characteristics vs. G_{m2} is then plotted in Fig. 9 (b), following the linear trend expressed in (9).

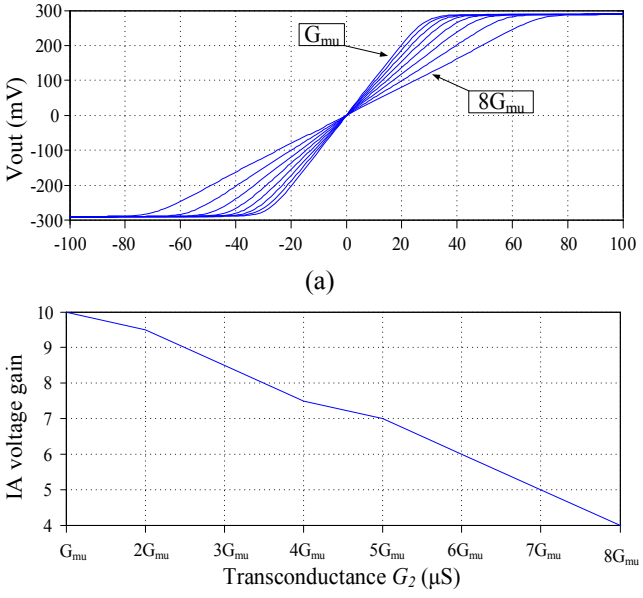

Figure 9. Variation of the IA voltage gain with G_2 equivalent transconductance value: (a) voltage transfer characteristics and (b) programming characteristics

Analog tuning of the IA voltage gain via the transconductor G_2 current divider M_{r1}-M_{r2} differential control voltage V_{cd} is illustrated in Fig. 10, with Fig. 10 (a) plotting the voltage transfer characteristics for various values of V_{cd} and Fig. 10 (b) plotting the programming characteristics of the IA voltage gain vs. V_{cd}.

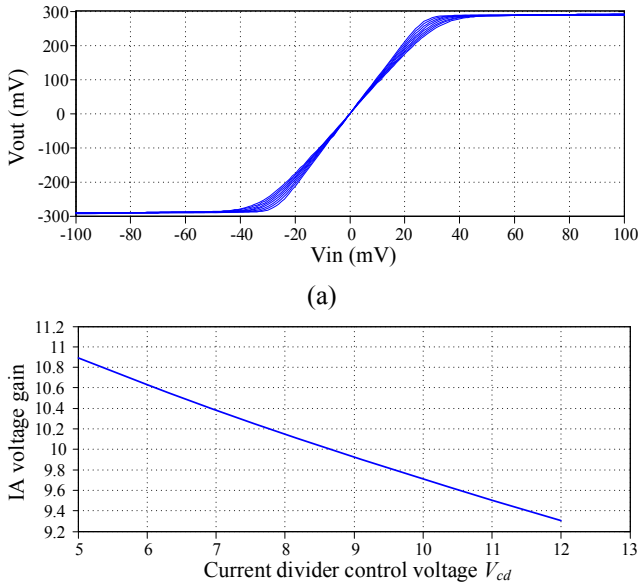

Figure 10. Analog tuning of the IA voltage gain with the M_{r1}-M_{r2} current divider differential control signal V_{cd}: (a) voltage transfer characteristics and (b) tuning characteristics

Simulation of the biopotential monitoring system analog front-end from Fig. 7 is illustrated further on. The analog front-end was configured for ECG signal monitoring, i.e. 0.05-100 Hz baseband frequency, as plotted in Fig. 11. A x1 IA gain was initially considered.

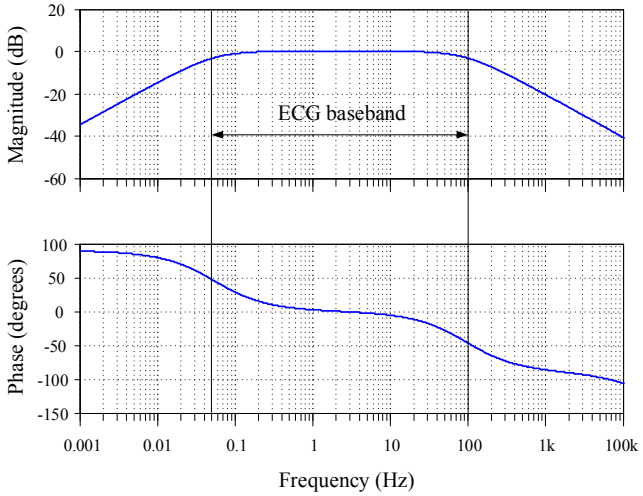

Figure 11. Frequency characteristics of the proposed IA configured for ECG signal monitoring

Tuning of the IA voltage gain is illustrated in the ECG baseband around the x100 reference voltage gain. Accordingly, M_{dr} was switched to the x100 reference voltage gain and G_2 was varied in the $4G_{mu}$ - $8\ G_{mu}$ range. The frequency characteristics are plotted in Fig. 12.

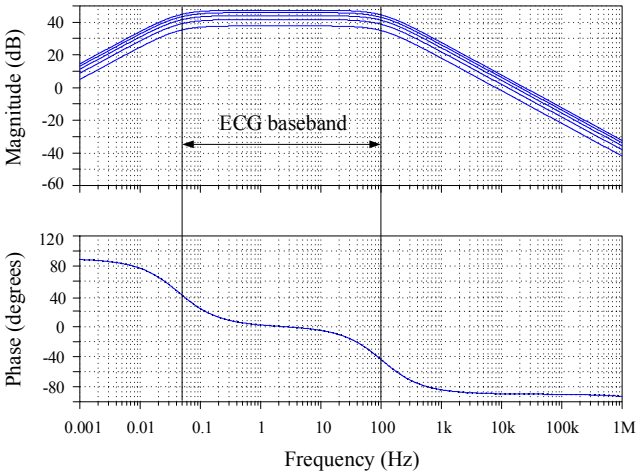

Figure 12. Frequency characteristics of the proposed IA configured for ECG signal monitoring

The frequency characteristics form Fig. 12 illustrate that, similarly to Fig. 9, digital programming of the IA voltage gain vs. G_2 follows the linear trend expressed in (9).

The programmability of the biopotential monitoring system analog front-end frequency-selective behavior is presented as follows. For fixed values of G_{m3}=G_{m4}, the filter lower cutoff frequency is plotted vs. the transconductance value in Fig. 13. Accordingly, digital programming of the frequency characteristics follows the variation trend expressed in (14).

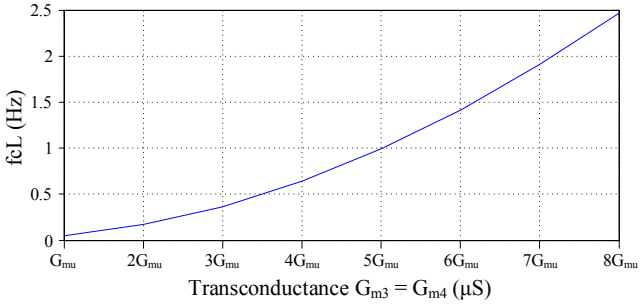

Figure 13. Variation of the IA lower frequency limit with Gm3= Gm4 equivalent transconductance values

Fine-tuning the filter lower cutoff frequency around the nominal value of 0.05Hz for ECG signal acquisition via the Mr1-Mr2 current divider of both transconductors Gm3 and Gm4 is plotted next in Fig. 14.

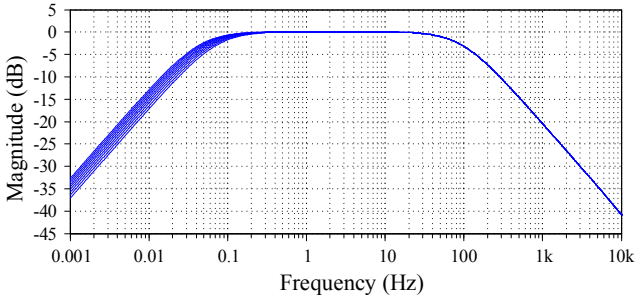

Figure 14. Tuning of the IA lower cutoff frequency around the 0.05Hz value with the equivalent width of M_{r2} switched parallel transistor arrays

VI. Conclusion

This paper proposed a fully-differential low-power resistance-free instrumentation amplifier for use in the analog front-end of bio-potential monitoring systems, with programmable frequency-selective behaviour. The proposed instrumentation amplifier was implemented around the current balancing technique and thus achieved increased flexibility. The passive resistances have been replaced with active equivalents, enabling integration in silicon by considerably reducing chip area. Accordingly, IA gain is set as the ratio of two transconductance values, rather than two resistance values as was the case in formerly reported solutions. Bulk input and bump-linearization were employed as linearization techniques to accommodate the required voltage swing. The proposed instrumentation amplifier exhibits two degrees of freedom to control the operation parameters. One degree of freedom sets the desired value of the operating parameters and the other is used for fine-tuning. Subthreshold biasing was employed to achieve low-power consumption. The instrumentation amplifier output stage was applied to a Gm-C bandpass Tow-Thomas biquad. Considering the rather large capacitance values, which require external components, a constant-C tuning technique was implemented for programming the biopotential monitoring front-end frequency-selective behaviour. The proposed circuits were validated using Cadence on a 0.35 µm CMOS process, thus demonstrating the applicability of the proposed solutions for programming the operation parameters to the amplitude and baseband specifications of particular bio-medical signals.

References

[1] L. Magnelli, F. A. Amoroso, F. Crupi, G. Cappuccino, G. Iannaccone, "Design of a 75-nW, 0.5-V subthreshold complementary metal-oxide-semiconductor operational amplifier", International Journal of Circuit Theory and Applications, vol. 42, no. 9, pp. 967-977, Sept. 2014. doi: http://dx.doi.org/10.1002/cta.1898

[2] F. Bautista, S.O. Martinez, G. Dieck, O. Rossetto, "An ultra-low voltage high gain operational transconductance amplifier for biomedical applications", in 2007 Workshop on Design and Architectures for Signal and Image Processing (DASIP), Grenoble, France, Nov 2007. hal id: http://hal.in2p3.fr/in2p3-00192566/en

[3] R. Sarpeshkar, Ultra Low Power Bioelectronics: Fundamentals, Biomedical Applications, and Bio-Inspired Systems. Cambridge University Press, 2010.

[4] R. Groza and M. Cirlugea, "Current-mode log-domain programmable gain amplifier," in 2014 IEEE International Conference on Automation Quality and Testing Robotics (AQTR), pp. 75-78, 2014. doi: http://dx.doi.org/10.1109/AQTR.2014.6857850

[5] V. Petkus, A. Preiksaitis, S. Krakauskaite, R. Chomskis, S. Rocka, A. Kalasauskiene, et al., "Novel Method and Device for Fully Non-Invasive Cerebrovascular Autoregulation Monitoring", Elektronika ir Elektrotechnika, vol. 20, no. 8, pp. 24-29, 2014. doi: http://dx.doi.org/10.5755/j01.eee.20.8.5464

[6] C. Rotariu, V. Manta, R. Ciobotariu, "Integrated System Based on Wireless Sensors Network for Cardiac Arrhythmia Monitoring," Advances in Electrical and Computer Engineering, vol.13, no.1, pp.95-100, 2013. doi:10.4316/AECE.2013.01016

[7] P. Farago, S. Hintea, F. Sandu, "A digital control mechanism for the delay of a dual-microphone analog beamformer", 2017 International Conference on Optimization of Electrical and Electronic Equipment (OPTIM) & 2017 Intl Aegean Conference on Electrical Machines and Power Electronics (ACEMP), ISBN 978-1-5090-4489-4, 2017. doi: 10.1109/OPTIM.2017.7975067

[8] J. H. Nagel, "Biopotential Amplifiers", in Ed. Joseph D. Bronzino, The Biopotential Engineering Handbook: Second Edition, CRC Press LLC, 2000.

[9] C.-C. Huang, C. Tung, S.-H. Hung, J.-F. Chung, L.-D. Van, C.-T. Lin, "Front-end amplifier of low-noise and tunable BW/gain for

portable biomedical signal acquisition", in IEEE International Symposium on Circuits and Systems, pp. 2717-2720, 2008. doi: http://dx.doi.org/10.1109/ISCAS.2008.4542018

[10] J. A. De Lima, "A compact low-distortion low-power instrumentation amplifier", in Proceedings of the 22st Annual Symposium on Integrated Circuits and Systems Design: Chip on the Dunes, SBCCI 2009, Natal, Brazil, August 31 - September 03, 2009. doi: 10.1145/1601896.1601931

[11] C. Kitchin, L. Counts, A Designer´s Guide to Instrumentation Amplifiers, 2nd Edition, Analog Devices, 2004.

[12] L. Fay, V. Misra, R. Sarpeshkar. "A Micropower Electrocardiogram Amplifier", IEEE Transactions on Biomedical Circuits and Systems, vol. 3, no. 5, pp. 1932-4545, 2009. doi: http://dx.doi.org/10.1109/TBCAS.2009.2026483

[13] R. Wu, K. A. A. Makinwa, J. H. Huijsing, "A Chopper Current-Feedback Instrumentation Amplifier With a 1 mHz 1/f Noise Corner and an AC-Coupled Ripple Reduction Loop", IEEE Journal of Solid-State Circuits, vol. 44, no. 12, 2009. doi: 10.1109/JSSC.2009.2032710

[14] T. Denison, K. Consoer, W. Santa, A. Avestruz, J. Cooley, A. Kelly, "A 2 μW 100 nV/rtHz Chopper-Stabilized Instrumentation Amplifier for Chronic Measurement of Neural Field Potentials", IEEE Journal of Solid-State Circuits, vol. 42, no. 12, pp. 2934 - 2945, 2008. doi: 10.1109/JSSC.2007.908664

[15] C.-H. Hsu, C.-C. Huang, K. Siong, W.-C. Hsiao, C.-C. Wang, "A high performance current-balancing instrumentation amplifier for ECG monitoring systems" in 2009 International SoC Design Conference (ISOCC), Busan, South Korea, 2009. doi: 10.1109/SOCDC.2009.5423877

[16] W.-Y. Huang, Y.-W. Cheng, K.-T. Tang, "A 0.5-V multi-channel low-noise readout front-end for portable EEG acquisition", in 2015 37th Annual International Conference of the IEEE Engineering in Medicine and Biology Society (EMBC), Milan, Italy, 2015. doi: 10.1109/EMBC.2015.7318492

[17] C.-Y. Wu, C.-S. Ho, "An 8-channel chopper-stabilized analog front-end amplifier for EEG acquisition in 65-nm CMOS", in 2015 IEEE Asian Solid-State Circuits Conference (A-SSCC), Xiamen, China, 2015. doi: 10.1109/ASSCC.2015.7387480

[18] J. Kim, H. Ko, "A Dynamic Instrumentation Amplifier for Low-Power and Low-Noise Biopotential Acquisition", Sensors, vol. 16, no. 3, pp. 354, 2016. doi:10.3390/s16030354

[19] R. Wu, J. H. Huijsing, K. A. A. Makinwa, Precision Instrumentation Amplifiers and Read-Out Integrated Circuits, Chapter 2, "Dynamic Offset Cancellation Techniques for Operational Amplifiers", pp. 21-49, Springer, New York, 2013. doi: https://doi.org/10.1007/978-1-4614-3731-4_2

[20] Y. Kusuda, "5.1 A 60V auto-zero and chopper operational amplifier with 800kHz interleaved clocks and input bias-current trimming", in 2015 IEEE International Solid- State Circuits Conference - (ISSCC), San Francisco, CA, USA, 2015. doi: 10.1109/ISSCC.2015.7062939

[21] F. Geusa, A. Agnes, F. Maloberti, "Use of chopper-notch modulator in chopper amplifiers for replica images cancellation" in 15th IEEE International Conference on Electronics, Circuits and Systems, St. Julien's, Malta, 2008. doi: 10.1109/ICECS.2008.4674916

[22] B. Dobkin, J. Williams, Analog Circuit Design - Volume 2, Elsevier, 2013.

[23] A. Worapishet, A. Demosthenous, X. Liu, "A CMOS Instrumentation Amplifier With 90-dB CMRR at 2-MHz Using Capacitive Neutralization: Analysis, Design Considerations, and Implementation", IEEE Transactions on Circuits and Systems I: Regular Papers, vol. 58, no. 4, pp. 699-710, 2011. doi: 10.1109/TCSI.2010.2078850

[24] R. Martins, S. Selberherr, F. Vaz, "A CMOS IC for portable EEG acquisition systems", in IEEE Instrumentation and Measurement Technology Conference, vol 2, pp. 1406-1410, 1998. doi: http://dx.doi.org/10.1109/IMTC.1998.676985

[25] C. Nanda, J. Mukhopadhyay, D. Mandal, S. Chakrabarti, "A CMOS instrumentation amplifier with low voltage and low noise for portable ECG monitoring systems", in IEEE International Conference on Semiconductor Electronics, pp. 54 - 58, 2008. doi: http://dx.doi.org/10.1109/SMELEC.2008.4770276

[26] P. Farago, M. Cirlugea, S. Hintea, "An electronically programmable current balancing instrumentation amplifier for biomedical monitoring", in 2016 39th International Conference on Telecommunications and Signal Processing (TSP), Vienna, Austria, 2016. doi: 10.1109/TSP.2016.7760876

[27] H. Wu, Y.-P. Xu, "A low-voltage low-noise CMOS instrumentation amplifier for portable medical monitoring systems", in The 3rd International IEEE-NEWCAS Conference, 19-22 June 2005, pp. 295-298. doi: http://dx.doi.org/10.1109/NEWCAS.2005.1496659

[28] M. S. J. Steyaert, W. M. C. Sansen, "A micropower low-noise monolithic instrumentation amplifier for medical purposes", IEEE Journal of Solid-State Circuits, vol. 22, no. 6, pp. 1163-1168, 1987. doi: http://dx.doi.org/10.1109/JSSC.1987.1052869

[29] J. Jerabek, J. Dvorak, R. Sotner, B. Metin, K. Vrba, "Multifunctional current-mode filter with dual-parameter control of the pole frequency", Advances in Electrical and Computer Engineering, vol.16, no.3, pp.31-36, 2016. doi:10.4316/AECE.2016.03005

[30] K. Garje, S. Kumar, A. Tripathi, G. Maruthi, M. Kumar, "A high CMRR, high resolution bio-ASIC for ECG signals" in 2016 20th International Symposium on VLSI Design and Test (VDAT), Guwahati, India, 2016. doi: 10.1109/ISVDAT.2016.8064890

[31] W.-C. Huang, K.-T. Tang, "A 90 nm CMOS low noise readout front-end for portable biopotential signal acquisition", in 2012 IEEE Biomedical Circuits and Systems Conference (BioCAS), Hsinchu, Taiwan, 2012. doi: 10.1109/BioCAS.2012.6418476

[32] S. Hintea, G Csipkes, D. Csipkes, L. Festila, R. Groza, P. Farago, M.Cirlugea, Reconfigurable Analog Circuits for Mobile Communications, Variable topology filters and design automation, Editura Casa cărţii de ştiinţă, 2011, pp. 202-208.

[33] E. Arslan, "Self-Biasing High Precision CMOS Current Subtractor for Current-Mode Circuits", Advances in Electrical and Computer Engineering, vol.13, no.4, pp.19-24, 2013. doi:10.4316/AECE.2013.04004

[34] P. Farago, C. Farago, G. Oltean, S. Hintea, "An Electronically Tunable Transconductance Amplifier for Use in Auditory Prostheses", Advances in Electrical and Computer Engineering, vol.15, no.4, pp.95-100, 2015. doi:10.4316/AECE.2015.04013

[35] S. Pavan, Y. P. Tsividis, K. Nagaraj, "Widely programmable high-frequency continuous-time filters in digital CMOS technology", IEEE Journal of Solid-State Circuits, vol. 35, no. 4, pp. 503-511, 2000. doi: http://dx.doi.org/10.1109/4.839910